applied sciences

MDPI

Article

Controlling Thermal Radiation in Photonic Quasicrystals Containing Epsilon-Negative Metamaterials

Ameneh Mikaeeli [1,2,*], Alireza Keshavarz [3], Ali Baseri [3] and Michal Pawlak [1,*]

[1] Institute of Physics, Faculty of Physics, Astronomy and Informatics, Nicolaus Copernicus University in Torun, Grudziadzka 5, 87-100 Torun, Poland
[2] Faculty of Physics and Astronomy, Ruhr-University Bochum, Universitaetsstrasse 150, D-44780 Bochum, Germany
[3] Departments of Physics, Shiraz University of Technology, Shiraz 71557-13876, Iran; keshavarz@sutech.ac.ir (A.K.); a.baseri@sutech.ac.ir (A.B.)
* Correspondence: ameneh.mikaeeli@doktorant.umk.pl (A.M.); mpawlak@fizyka.umk.pl (M.P.)

Abstract: The transfer matrix approach is used to study the optical characteristics of thermal radiation in a one-dimensional photonic crystal (1DPC) with metamaterial. In this method, every layer within the multilayer structure is associated with its specific transfer matrix. Subsequently, it links the incident beam to the next layer from the previous layer. The proposed structure is composed of three types of materials, namely InSb, ZrO_2, and Teflon, and one type of epsilon-negative (ENG) metamaterial and is organized in accordance with the laws of sequencing. The semiconductor InSb has the capability to adjust bandgaps by utilizing its thermally responsive permittivity, allowing for tunability with temperature changes, while the metamaterial modifies the bandgaps according to its negative permittivity. Using quasi-periodic shows that, in contrast to employing absolute periodic arrangements, it produces more diverse results in modifying the structure's band-gaps. Using a new sequence arrangement mixed-quasi-periodic (MQP) structure, which is a combination of two quasi periodic structures, provides more freedom of action for modifying the properties of the medium than periodic arrangements do. The ability to control thermal radiation is crucial in a range of optical applications since it is frequently unpolarized and incoherent in both space and time. These configurations allow for the suppression and emission of thermal radiation in a certain frequency range due to their fundamental nature as photonic band-gaps (PBGs). So, we are able to control the thermal radiation by changing the structure arrangement. Here, the We use an indirect method based on the second Kirchoff law for thermal radiation to investigate the emittance of black bodies based on a well-known transfer matrix technique. We can measure the transmission and reflection coefficients with associated transmittance and reflectance, T and R, respectively. Here, the effects of several parameters, including the input beam's angle, polarization, and period on tailoring the thermal radiation spectrum of the proposed structure, are studied. The results show that in some frequency bands, thermal radiation exceeded the black body limit. There were also good results in terms of complete stop bands for both TE and TM polarization at different incident angles and frequencies. This study produces encouraging results for the creation of Terahertz (THz) filters and selective thermal emitters. The tunability of our media is a crucial factor that influences the efficiency and function of our desired photonic outcome. Therefore, exploiting MQP sequences or arrangements is a promising strategy, as it allows us to rearrange our media more flexibly than quasi-periodic sequences and thus achieve our optimal result.

Keywords: thermal radiation; photonic crystal; metamaterial; terahertz filter

Citation: Mikaeeli, A.; Keshavarz, A.; Baseri, A.; Pawlak, M. Controlling Thermal Radiation in Photonic Quasicrystals Containing Epsilon-Negative Metamaterials. *Appl. Sci.* **2023**, *13*, 12947. https://doi.org/10.3390/app132312947

Academic Editor: Bahram Djafari-Rouhani

Received: 17 October 2023
Revised: 23 November 2023
Accepted: 30 November 2023
Published: 4 December 2023

1. Introduction

Photonic crystals (PCs), originally proposed by Yablonovitch, are intricate structures composed of layers consisting of dielectric and/or other materials. These layers are organized in periodic, quasi-periodic (QP), or combinations of both configurations, endowing

PCs with remarkable capabilities for precision control, management, and the manipulation of incident light beams. This unique property arises from the phenomenon known as the PBG [1–6]. The PBG inhibits electromagnetic (EM) waves from propagating within specific frequency bands and length scales, an effect rooted in the interference of Bragg scattering within periodic structures. In addition to their role in optical control, PCs offer intriguing possibilities for modifying thermal radiation processes. Thermal radiation, characterized by spontaneous emission driven by the inherent fluctuations of atoms and particles, reaches thermal equilibrium with its surroundings. This equilibrium condition serves as the foundation for substantial alterations to Planck's black-body radiation spectrum. These modifications hinge on optimizing the coupling between the multi-mode radiation field within a PC and a collection of emitters. It is worth noting that, per the fundamental principle defining blackbody objects, the thermal flux emitted by any material object for any given frequency and direction cannot surpass that of a black body at the same temperature within identical surroundings [7–10]. PCs have been extensively employed in two predominant structural arrangements: absolute periodic and quasi-periodic (QP) configurations. These optical properties of such media are now well established. In addition to their scientific significance, these versatile structures hold immense potential for a diverse array of technological applications, encompassing thermophotovoltaic energy conversion devices, advanced light sources, THz filters, and adaptable thermal emitters. Absolute periodic media, characterized by the repetitive recurrence of constituent elements and layers with strict periodicity, offer limited flexibility for structural adaptations despite yielding some valuable results. In contrast, quasi-periodic media, where structures do not adhere to strict periodicity, provide greater freedom for structural adjustments. These quasi-periodic arrangements adhere to specific mathematical relationships, including but not limited to the Fibonacci series (FB), Thue–Morse (T-M) sequence, maximum length (ML) sequence, fractals triadic, double period (DP), and others. Although not strictly ordered, these arrangements conform to underlying regular and mathematical principles [11–18].

Moreover, the integration of negative refractive index materials (NRIMs) or metamaterials within PC structures has garnered significant attention in recent years. These artificial materials, usually characterized by negative permittivity and permeability, alter the behavior of EM waves in novel ways. Despite the presence of positive index materials (PIMs), NRIMs facilitate the propagation of Poynting and wave vectors in opposing directions, making them particularly intriguing for thermal radiation modulation [19,20]. The pioneering work of Maksimovic et al. applied periodic and quasi-periodic (QP) structures containing both PIMs and NRIMs to achieve thermal radiation modulation, sparking numerous investigations in the field. Numerous investigations into the field of research have been conducted since then [21–23]. The evolution of metamaterial-based sciences has been instrumental in propelling progress across diverse disciplines, encompassing photonics, material science, nanotechnology, THz technology, thermodynamics, electronics, acoustics, and beyond. This interdisciplinary impact underscores the profound implications of metamaterial research on a broad spectrum of scientific and technological domains. It is worth mentioning that not all types of metamaterials exhibit a negative refractive index. A necessary condition for achieving a negative refractive index is that both permittivity and permeability have negative values [24,25]. However, some metamaterials, such as ENG and mu-negative (MNG), can also display a negative refractive index in certain frequency domains.

For the ENG metamaterial that we used in our media, it only has a negative permittivity, so the resulting refractive index is positive. It is also important to note that the ENG metamaterial introduces loss due to its negative permittivity and its complex refractive index. This is actually desirable for our proposed structure because this loss enables the medium to store more energy, which facilitates radiation.

In this study, we investigate the power spectrum of the suggested multilayer structure's thermal radiation using a novel type of configuration called MQP arrangement [26]. In this arrangement, different types of QP arrangement could be utilized as follows; Fibonacci (FB),

maximum length (ML), Thue–Morse (T-M), and double period (DP) sequences. See [27] for additional information on QP configurations. The MQP structures have additional flexibility in how their components are configured. As a result, the MQP arrangement may be a viable choice for designing our desired thermal emitter in accordance with our goals. Effective thermal management is essential for diverse devices, with some requiring low thermal radiation to prevent overheating, such as electronics, satellites, and medical equipment. On the other hand, devices like thermal power plants, solar absorbers, and heating elements benefit from high thermal radiation to optimize energy efficiency and heat generation. The use of MQP arrangements allows for enhanced tunability in controlling thermal radiation within desired frequency ranges, providing a versatile solution to meet the specific thermal needs of different applications. Various thermal radiation PBG structures could be created using MQP arrangements. By using the arrangements in specific frequency ranges, the structures could be flexibly tuned and manipulated, and the thermal radiation could be effectively raised up to the black-body limitations. The proposed structure is a combination of FB and ML sequences. The transfer matrix method (TMM) [28] is used to give numerical findings for study and calculation in MATLAB (R2023b-academic use) software.

Regarding the alternative models, which could potentially be used instead of the TMM, several models could be mentioned to be discussed such as RCWA, which this method is discussed earlier, finite difference time domain (FDTD) [29], and spectral domain method (SDM) [30], etc. In an exact and perfect comparison, it will clearly be inferred that among those models the TMM is the more accurate, practical, easiest to use, and efficient model that could be applied to our study, which concerns the transmission, reflection, and radiation quantities in a 1DPC medium, due to the following reasons: On the one hand, the TMM can handle arbitrary incidence angles and polarization states in 1DPCs. This model is superior in calculating the reflection and transmission coefficients of a 1DPC. Furthermore, the TMM can easily incorporate dispersion and loss in the materials. On the other hand, the FDTD method is more versatile and requires more computational resources and time [31]. Working with this model is more complex since it divides the computational domain into a grid of cells and updates the electric and magnetic fields at each cell using discrete approximations of the curl equations. The SDM also requires a large number of Fourier modes to achieve good accuracy, especially for high-contrast structures and oblique incidence angles [32], whereas TMM only requires a few matrix multiplications to obtain the same accuracy. Moreover, SDM is limited to normal incidence and TE or TM polarization. As a consequence, TMM is significantly appropriate for studying one-dimensional structures, such as multilayer films, Bragg gratings, Fabry–Perot resonators, and 1DPC and PBG structures.

The findings of this study, which investigates the thermal power spectra of electromagnetic radiation via 1DPC structure configurated by MQP arrangement, can help to design and fabricate novel devices for thermal energy harvesting and management, such as thermophotovoltaic cells, thermal switches, thermal diodes, and thermal transistors. It can also help to explore and manipulate the thermal radiation phenomena in MQP structures, such as surface modes, selective emission, and thermal rectification.

2. Materials and Methods

2.1. Submission

For the proposed structure, we calculate the transmission and reflection, denoted as T and R, respectively, as functions of both the incident wave's frequency (represented by ω) and its wave vector (k). In the case of a crystal with real refractive indices and no absorption or gain, energy conservation dictates that $R + T = 1$.

However, when absorption is present (corresponding to a complex refractive index), an absorption coefficient emerges and maintaining energy conservation is required. Furthermore, Kirchhoff's second law establishes a direct relationship between a material's thermal emittance, denoted as E, and its absorbance. Specifically, emittance is proportion-

ate to absorbance. In the case of a perfect blackbody thermal element, emittance equals absorbance. In this context, we have [33]

$$E(\omega) = A(\omega) = 1 - R(\omega) - T(\omega). \tag{1}$$

By multiplying the emittance by the Planck power spectrum $\rho^{BB}(\omega,\ Temp)$, the power spectrum of the proposed multilayer structure is given in terms of angular frequency and temperature as follows [33]:

$$\rho(\omega, Temp) = E(\omega)\rho^{BB}(\omega,\ Temp). \tag{2}$$

where $\rho^{BB}(\omega, Temp)$ is defined as follows:

$$\rho^{BB}(\omega,\ Temp) = \frac{\omega^2}{2c^2}\frac{\hbar\omega}{e^{\frac{\hbar\omega}{K_B T}} - 1}. \tag{3}$$

Here, $Temp = 1/(K_B T)$, and K_B is Boltzmann constant. c is the speed of light in free space, and $\hbar$ is known as Planck's constant divided by 2π. To derive the thermal power spectrum, Equations (1) and (2) state that the structure's transmission and reflection must be obtained.

Equation (1) represents the energy conservation principle for our proposed 1DPC structure. According to this equation, the incident radiation *E(ω)* splits into two parts, which have the same total energy as the incident radiation: the reflected wave $R(\omega)$ and the transmitted wave $T(\omega)$. The absorbed radiation $A(\omega)$ is the portion of the incident energy that is neither reflected nor transmitted, and it varies with the angular frequency ω of the radiation [34]. Equation (2) shows Kirchhoff's law of thermal radiation for the proposed medium. This law means that the structure's emission and absorption of radiation are balanced, depending on its temperature and frequency. The emissivity $E(\omega)$ of the structure is the fraction of radiation that it emits relative to a black body, which is an ideal emitter. The absorptivity $A(\omega)$ of the structure is the fraction of radiation that it absorbs from the incident radiation. These two fractions are the same for the proposed medium [35]. Since it is obvious that both the emissivity and the absorptivity are functions of the angular frequency (ω) and the angle of emission of the radiation.

A body in thermodynamic equilibrium emits electromagnetic radiation, which is subject to Kirchhoff's law of thermal radiation. The power spectrum is a way of showing how much power or energy the radiation has at different frequencies. The power spectrum can be found using Planck's law of black-body radiation, which tells the spectral radiance of a body at a given temperature and wavelength [9]. Regarding our proposed multilayer structure, there could be two thermal sources; thermal sources which originated from our THz incident beam, and from the applied external temperature. In accordance with the above explanation, after a thermodynamic equilibrium, the power spectrum quantity can be calculated using Planck's law of black-body radiation, emittance, and the Planck power spectrum quantities.

FB sequences consist of layers labeled as A and B. The l^{th} order of the QP structure, using the FB sequence is determined by $S_l = \{S_{l-2} - S_{l-1}\}$; $S_0 = \{B\}$, $S_1 = \{A\}$. Table 1 shows the multilayer structures created using the Fibonacci sequence, including configurations up to the 7th order. Moreover, ML sequence is a binary pseudo-random sequence with a length of $2^n - 1$, where n is an integer, which is shown in Table 2. Utilizing an ML involves designating a D layer (perturbation) whenever the ML assumes a unit value and a C layer when the sequence adopts a zero value. Regarding exploiting quasi-periodic sequences in photonic layered media, both FB and ML have been separately used in similar research. The effective impact of such sequences is that the photonic media no longer has to follow an absolutely periodic arrangement. By using, for example, FB sequence, although that photonic medium could be considerably configured, its element is just bound to this sequence. So, we can say the elements of that medium are just restricted to the FB sequence.

If we use the MQP sequence, we no longer have to bind ourselves just to a sequence. By doing so, our medium could benefit from many other mathematical sequences in a mixed but lawful and retrievable condition. Thus, among too many configuration statuses, we could choose an arrangement that matches our outcome of interest. More specifically, regarding using the FB and ML sequences, by using these arrangements in companion to each other, among many configuration statuses, we found an efficient arrangement to fulfill our purposes regarding the radiation PBGs in a practically easy-to-use and retrieve way of configuration.

Table 1. The configuration involves two distinct layers, designated as A and B, arranged in various sequences of the Fibonacci series.

Symbol	No. of Layer	Fibonacci Layer Sequence
S_0	1	B
S_1	1	A
S_2	2	BA
S_3	3	ABA
S_4	5	BAABA
S_5	8	ABABAABA
S_6	13	BAABAABABAABA
S_7	21	ABABAABABAABAABABAABA

Table 2. The configuration involves two distinct layers, designated as C and D, arranged in various sequences of the maximum length series.

Symbol	No. of Layer	Maximum Length Layer Sequence
S_0	1	D
S_1	2	DC
S_2	4	DCCD
S_3	7	DCCDCDC
S_4	12	DCCDCDCCDCCD
S_5	19	CCDCDCCDCCDCDCCDDC
S_6	28	CCDCDCCDCCDCDCCDDCCDCCDDCDC

The schematic of the proposed structure which is combination of QP sequences FB and ML is shown in Figure 1. The whole structure is composed of a 5th-order FB sequence and a 3rd-order ML sequence.

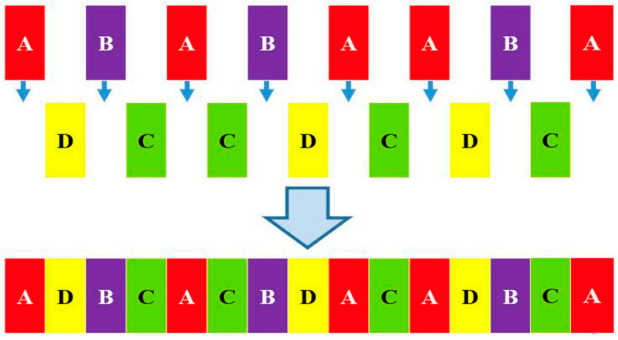

Figure 1. The geometrical representation of a one-dimensional multilayer structure containing ENG materials.

2.2. Transfer Matrix Method

The TMM is a technique that can be applied to study the transmission and reflection of EM or acoustic waves in a layered medium, such as a multilayer thin film structure [36]. This method is beneficial for determining the optical characteristics of 1DPCs, investigating

the behavior of acoustic waveguides and filters, modeling surface plasmon polaritons and metamaterials, designing anti-reflection coatings and dielectric mirrors, and more [37]. Another method that can be used to analyze the propagation of waves in a layered media is the rigorous coupled-wave analysis (RCWA) [38]. TMM is the easiest way to analyze and evaluate the behavior of the transmittance, reflectance, and radiation in proposed 1DPC structure as it defines a corresponding matrix for each layer of the media. A brief description of the RCWA is that it relies on the expansion of the electromagnetic field into the Fourier series and the application of the boundary conditions at the interfaces among different media [39]. Thus, we can conclude that the RCWA is more suitable for modeling the complex structures of gratings, PCs, and metamaterials, which are not easily handled by the TMM. To obtain the numerical results (transmission, reflection, and radiation) of our proposed 1DPC, we need to use the TMM to calculate the total transfer matrix of our media. This can be carried out by multiplying the transfer matrices of each component (layer) of our media. In the context of the interaction between an electromagnetic (EM) wave and the superlattice, the transfer matrix method (TMM) becomes a valuable tool for calculating the transmittance and reflectance of the entire structure. When an EM wave enters the 1DPC structure from the background medium at an incident angle θ, considering the refractive index variations along the z-direction of its layers, the relationship between the input and output of the EM wave can be expressed through the following transfer matrix.

Depending on the desired applications, 1DPC structure can be utilized in various novel devices, such as PC fibers, waveguides, microcavities, PC lasers, and more [40]. More specifically, advantages of thermal radiation in 1DPCs could be thermal energy harvesting [41], thermal sensing, thermal management [14], etc. The proposed structure has a wide range of market applications, but it requires further development and commercialization. The structure can be adapted and refined for each application by exploiting MQP arrangements. This could create a competitive edge in the field. The semiconductor InSb as layer A, Teflon as dielectric layer B, ENG metamaterial (containing thin wires) as layer C, and another type of dielectric ZrO_2 as layer D create the combinational structure of FB and ML sequences in the form of $(ADBCACBDACADBDB)^M$ shown in Figure 1. Here, layers A and B follow the 5th order of the FB sequence, and layers C and D follow the 3rd order of the ML sequence, respectively. The proposed structure is considered to be in a vacuum or air environment to compute the transmission, reflection, and absorption coefficients using the transfer matrix method. As shown in Figure 1, a beam of unit amplitude plane waves enters the structure with the incident angle θ from the air (left-hand side of the structure) and escapes via the structure from the right-hand side with its associated electric and magnetic fields. The transfer matrix of the j^{th} layer, which relates the electric and magnetic components of the incident beam at the left and right interfaces of the j^{th} layer, is given as follows [33]:

$$M_j = \begin{pmatrix} \cos(k_{jz}d_j) & -ip_{jz}^{-1}\sin(k_{jz}d_j) \\ -ip_{jz}\sin(k_{jz}d_j) & \cos(k_{jz}d_j) \end{pmatrix}. \quad (4)$$

where d_j ($j = A,\ B,\ C$ or D) is the thickness of j^{th} layer, $k_{jz} = (\omega/c)\sqrt{\varepsilon_j\mu_j}\sqrt{1-\left(\sin^2\theta/\varepsilon_j\mu_j\right)}$ is the z component of local wave vector in j^{th} layer, ω indicates the angular frequency of the incident wave, and Equations (5) and (6) represent the parameters associated with the transfer matrix for TE and TM modes, respectively:

$$P_{jz} = \sqrt{\frac{\varepsilon_j}{\mu_j}}\sqrt{1-\left(\sin^2\theta/\varepsilon_j\mu_j\right)}. \quad (5)$$

$$P_{jz} = \sqrt{\frac{\mu_j}{\varepsilon_j}}\sqrt{1-\left(\sin^2\theta/\varepsilon_j\mu_j\right)}. \quad (6)$$

The total transfer matrix of the multilayered structures is obtained by multiplying the corresponding matrix of each individual layer defined as

$$M_{Total} = \prod_{j=1}^{N} M_j = \begin{bmatrix} M_{11} & M_{12} \\ M_{21} & M_{22} \end{bmatrix}. \quad (7)$$

Accordingly, the transmission and reflection coefficients can be derived as Equations (8) and (9):

$$t(\omega) = \frac{2p_i}{(M_{11} + p_F M_{12})p_i + (M_{21} + M_{22}p_F)}. \quad (8)$$

$$r(\omega) = \frac{(M_{11} + M_{12}p_F)p_i - (M_{21} + M_{22}p_F)}{(M_{11} + M_{12}p_F)p_i + (M_{21} + M_{22}p_F)}. \quad (9)$$

where p_i and p_F are relevant to the initial and final environment corresponding to air $\varepsilon_i = \varepsilon_F = \varepsilon_0$. Therefore, $\mu_i = \mu_F = \mu_0$ and $p_i = p_F = \sqrt{\varepsilon_0/\mu_0}$ for TE and TM polarization, respectively. Subsequently, the total transmission and reflection can be reached as follows:

$$T(\omega) = \frac{p_F}{p_i}|t(\omega)|^2, R(\omega) = |r(\omega)|^2. \quad (10)$$

Regarding the dielectric layers Teflon and ZrO_2, both materials have unique optical properties, such as high transparency in the visible, near-infrared (NIR), and THz regions, low refractive index, and low absorption coefficient [42,43]. It can be used as an optical or photonic material for lenses, filters, waveguides, coatings, and substrates. Teflon is a synthetic polymer that has many benefits for various purposes. It has low friction, high strength, and excellent electrical insulation. It can resist high heat, strong chemicals, and corrosion [42]. ZrO_2 or Zirconia is a type of ceramic oxide that has remarkable properties. It has a high melting point, which means it can endure high temperatures. It has chemical stability, which means it does not react easily with other substances. It has mechanical strength, which means it can resist deformation and fracture. ENG metamaterials are artificial structures that could also exhibit negative effective permittivity. Arrays of metal rods that are covered with dielectric materials can be used to make ENG metamaterials. Dielectric materials are materials that can be polarized by electric fields. These arrays can produce plasmonic resonances and strong electric polarization. Plasmonic resonances are the collective vibrations of the electrons in the metal rods that are excited by the electric field of the light [44]. The effective parameters of such metamaterials depend on the geometry and material properties of the rods, as well as the frequency and polarization of the incident waves. High transparency in the infrared (IR) region, and strong magneto-optical effects are the photonic properties of InSb. It can specifically be used for THz and IR spectral filtering, nonreciprocal surface plasmon polaritons, and quantum nanostructures [45,46]. Plus, it also has high conductivity and thermal tunability, which can be exploited for sensing, switching, and modulating applications.

The refraction index of all the elements could be calculated by $n_i = \pm\sqrt{\varepsilon_i \mu_i}$ [47] according to the refraction index definition. Regarding signs $\pm$, if both ε_i and μ_i are negative quantity, then n_i takes sign $-$; otherwise, sign + assigned to n_i. Therefore, this relation takes sign $-$ just in the case of double-negative (DNG) metamaterial, and all the material utilized in the proposed structure takes sign +. It is also worth indicating that as all the materials are classified as diamagnetic or paramagnetic material, which means that they have no permanent magnetic moments and there is only a weak (negligible) induced magnetic response to the external magnetic field, their magnetic permeabilities were considered 1. Of course, it would be noticed that ENG and MNG metamaterials could also show negative refractive index over some frequency range.

3. Numerical Results and Discussion

3.1. Temperature Dependance of the Semiconductor Permitivity

InSb, a semiconductor with tunable permittivity in the THz frequency spectrum, plays a pivotal role in the proposed structure. Specifically, we focus on the unique tunability, arrangements, and properties of InSb for our investigation. Notably, InSb is utilized in its undoped form, a deliberate choice driven by specific considerations. In intrinsic InSb, the narrow bandgap between the conduction and valence bands (0.18 eV at room temperature) enables the unrestricted movement of charge carriers. By adjusting the external temperature, the intrinsic carrier density (N) can be precisely controlled. In contrast, lightly and moderately doped semiconductors tend to exhibit significant absorption of THz radiation by free carriers. To minimize the loss of the transmitted THz incident beam, this study strictly adheres to the use of undoped InSb. Within the specified frequency and temperature ranges, we accurately describe InSb's permittivity using the Drude model, which is presented as follows in our analysis [28]:

$$\varepsilon_A(\omega) = \varepsilon_\infty - \frac{\omega_{ps}^2}{\omega^2 + i\gamma\omega}\,. \tag{11}$$

where $\varepsilon_\infty = 15.68$ denotes the static dielectric constant. $\omega_{ps} = \sqrt{Ne^2/\varepsilon_0 m^*}$, and γ are relevant to the plasma frequency and damping constant, respectively. Here, e is the electronic charge, $m^* = 0.015m_e$ is the effective mass, where $m_e = 9.1 \times 10^{-31}$, and N (in cm^{-3}) is the intrinsic carrier density, which demonstrates the dependence of ω_{ps} and, eventually, the permittivity of InSb on temperature by given relation as follows:

$$N = 5.67 \times 10^{14} Temp^{\frac{3}{2}} exp\left(\frac{-0.13}{k_B Temp}\right). \tag{12}$$

where $Temp$ refers to the temperature in Kelvin. Here, all the evaluations are performed based on a particular temperature. As evident from Equations (11) and (12), the permittivity of InSb is temperature dependent; thus, it facilitates our objectives regarding the thermal tunability of the proposed structure. Despite the limitations and inaccuracies of the Drude model, describing the permittivity of InSb in the THz frequency range by this model could be advantageous due to the following reasons [48]. First, this model explains the dependence of the permittivity on the temperature and magnetic field. Plus, it is suitable for describing the interaction of geometrical light with the 1DPC medium to predict the reflection, transmission, and absorption spectra of the 1DPC, as well as the thermal emission and the PBG. More importantly, this model can also be easily incorporated into the transfer matrix method, which is a common numerical technique for analyzing the optical properties of 1DPCs. According to the aforementioned relations, it could be noticed that InSb's intrinsic carrier density considerably depends on the temperature. Plus, this dependency has a direct effect on the plasma frequency and permittivity. Therefore, the variation in temperature causes the variation in permittivity and refractive index of InSb. This change in the refraction index leads to a new difference path inside the proposed photonic medium; thus, temperature tunability could be achieved.

The ENG metamaterial can considerably tune our PBGs and manipulate the incident waves. In truth, changing the lattice constant corresponding to the applied ENG metamaterial can make our structure efficiently tunable toward the lattice constants. Furthermore, the dependency of its refractive index on the frequency amounts also makes our medium tunable towards the frequency domains. More importantly, the damping in our structure, which is mainly caused by our ENG metamaterial due to its complex refractive index, helps us to have a more efficient radiation spectrum. Metamaterials are categorized and named

in accordance with the sign of their permittivity and permeability. The permittivity of the ENG metamaterials is given by [49]

$$\varepsilon_C(\omega) = 1 - \frac{\omega_{pm}^2}{\omega(\omega + i\Gamma)}. \tag{13}$$

$$\omega_{pm} = \sqrt{\frac{2\pi c^2}{a^2 ln\left(\frac{a}{r}\right)}}. \tag{14}$$

Here, ω_{pm} represents the plasma frequency, $\Gamma = 2\pi(0.08\ \text{THz})$ is the dissipation coefficient of the ENG construction, and a = 50 µm and r = 1 µm indicate the length and radius of the cross-section of the wires, which exist in our ENG metamaterial, respectively. Ref. [50] has further information about ENG and other types of metamaterials.

3.2. External Temperature

First of all, it is worth mentioning that the tunability in such a PC medium is considered a highly practical advantage. The more tunable this device, the better it can optimally be utilized in the applications of interest under the desired conditions. Secondly, as this device could also be exploited in thermos optical usages like thermal energy harvesting and management, thermal switches, transistors, etc., the thermal tunability of the proposed structure could pave the way for an efficient performance of that optical device. In the far-infrared (FIR) range of the THz spectrum, the temperature-dependent permittivity, $\varepsilon_C(\omega)$, of InSb exhibits remarkable sensitivity to variations in temperature. This sensitivity gives rise to intriguing and anomalous optical features in 1DPCs composed of InSb and a dielectric material. The temperature dependence is shown in Figure 2 for both real and imaginary parts. In this figure, the temperature varies between 150 K and 250 K. At low temperatures, roughly ranging from 150 K to 200 K, the permittivity dispersion is relatively weak, resulting in both the real and imaginary parts of $\varepsilon_C(\omega)$ being positive. However, as temperatures rise, the real part of $\varepsilon_C(\omega)$ can exhibit both positive and negative values, while the imaginary part remains consistently positive. Consequently, manipulating the tunability of $\varepsilon_C(\omega)$ could serve to achieve a temperature-dependent composite. The numerical data clearly depict the proposed structure's temperature dependency as follows. The transmittance spectrum of the structure at three different temperatures under the usual incoming beam is shown in Figure 2a–c. The lattice constants are $d_A = 28$ µm, $d_B = 12$ µm ($\varepsilon_B = 2.1$ $\mu_B = 1$), $d_C = 3$ µm, and $d_D = 12$ µm ($\varepsilon_D = 4.41$ $\mu_D = 1$). Additionally, the damping coefficients are considered to be $\gamma = 0$ and $\Gamma = 0.034$ THz. Also, the number of periods is $M = 4$. As shown in Figure 2, increasing the applied external temperature causes the PBGs to shift towards higher frequencies. This event demonstrates that the transmittance spectrum is temperature adjustable. For example, the mean frequency point of band-gap I is 0.10 THz with a width of 0.21 THz at T = 150 K, while the mean frequency point and the width of gap III are 0.09 THz and 0.19 THz at T = 250 K, respectively. However, the change is not significantly noticeable, and all of the lower and upper frequency limits of the band-gaps are shifted towards the higher frequency by increasing the temperature. Complete gaps, which totally stop the propagation of the incident beam through the structure, can be shown in Figure 2. At lower frequencies, the band-gaps are practically as narrow as they are at higher frequencies. As a result, the width can be adjusted according to the frequency.

The above analysis indicates that a THz mirror can be achieved within multilayer structures comprising the semiconductor material InSb. The upper and lower band-edge frequencies, as well as the bandwidth of the PBG, can be adjusted by modifying the external temperature. THz mirrors play a significant role in future THz communication systems.

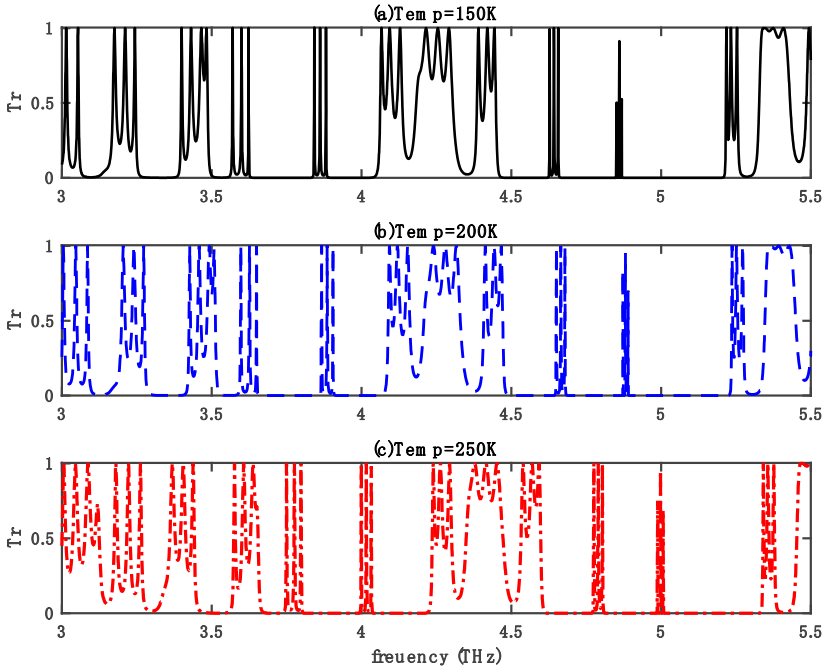

Figure 2. The transmittance spectrum of the 1D MQP PC, consisting of layers A = InSb, B = Teflon, C = ENG and D = ZrO_2 (with FB and ML arrangements), is plotted as a function of frequency. The thicknesses of the layers are $d_A = 28$ µm, $d_B = 12$ µm, $d_C = 3$ µm, and $d_D = 12$ µm, and the number of periods is $M = 4$ under the normally incident beam at different temperatures T = (**a**) 150 K, (**b**) 200 K and (**c**) 250 K.

3.3. Incident Angle

Because the incidence angle may effectively adjust the thermal radiation spectrum, the developed structure could be used as a selective thermal emitter in the THz regime [51]. As it is significant for a range of applications, and adjusting the incidence angle contributes by enabling directional emission, tuning emission spectra, and providing dynamic control over the thermal radiation. These capabilities enhance the versatility and effectiveness of THz technology in various fields. The examination of the structure's angular thermal radiation is consequently important in this case. According to the Fresnel Law, the angle of the incident can change the resultant thermal radiation. So, the direction of the incident beam which will be separated into two TE and TM modes can significantly affect the consequent radiation. Moreover, as thermal radiation is spatially incoherent, employing such periodic structures enables us to control the amount of thermal radiation in specific frequency ranges, i.e., increase, decrease, or completely stop it.

The achieved power spectrum (radiance) curves in Figure 3 demonstrate some PBGs, as well as a well-behaved frequency region as maximum radiance, for the TE polarized wave under different incident angles. According to Figure 3, the maximum thermal radiation occurs at any angle of the incident beam. As shown, the maximum radiation range, of which the radiance value reaches 1, is considered from 3.63 THz to 4.73 THz $\theta = 0$, with the width $\Delta f = 1.1$ THz. As the θ increases, the width of maximum thermal radiation becomes wide and wider, insofar as the width reaches Δf =1.45 THz at $\theta = 85°$. Furthermore, the maximum range moves towards upper frequencies as θ increases. It is obvious in the figure that the frequencies of the upper band-edges moves faster than the frequencies of the lower band-edges when θ increases. As demonstrated in Figure 3, two PBGs emerged in the radiance spectrum as Gaps I and II, which are also tuned by the incidence angle changes. For example, Gap I is placed at 3.4 THz for θ = 0, while it is placed at 3.63 THz for $\theta = 85°$. On the other hand, the radiance minimum value of Gap II reaches zero by increasing the incidence angle so that the gap becomes a complete PBG at $\theta = 85°$. The most remarkable property in Figure 3 relates to the dashed rectangular area on the

maximum thermal radiation ranges. Here, the radiation spectrum remains invariant in the frequency range $f_a = 3{\cdot}97$ THz to $f_b = 4{\cdot}51$ THz (Δf =0.57 THz), with an increase in the incident angle from 0° to 85°, such type of the spectra is called the omnidirectional spectrum.

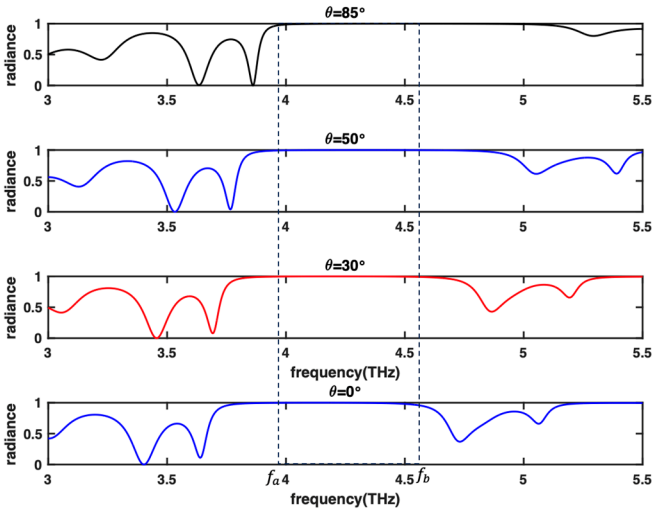

Figure 3. The thermal radiation power spectrum (dashed rectangle depicts the omnidirectional spectrum) of the 1D MQP PC (with FB and ML sequences) as a function of frequency for TE polarization at T = 300 K and M = 1, under several incident angles $\theta = 0°$, 30°, 50°, and 85°. Here, the lattice constants are considered as $d_A = 12$ µm, $d_B = 6$ µm, $d_C = 8$ µm, and $d_D = 6$ µm.

As shown in Figure 4, the thermal radiation spectrum of both incident TM polarized waves is plotted in terms of frequency at angles $\theta = 0°, 30°, 50°, 85°$. It is clear in that only the upper-frequency limits of the band-gaps are significantly sensitive to increasing the angles of incident, while for the lower frequency limits these changes are very small. Figure 4 shows a TM polarization plot of the light under identical conditions as shown in Figure 3. The relevant analysis is described as follows. Similar to Figure 3, by increasing the angle of incidence frequency limits of the PBGs move to the higher frequencies. For example, we can see the lower band-edge is occurred at 3.64 THz for $\theta = 0°$ as the TE mode. As the angle increases to $\theta = 30°$ and $\theta = 50°$, the lower edges occur at frequencies 3.80 THz and 4.09 THz, respectively. It is obvious that the lower edges moved to the higher frequencies, but the movement is faster than the TE polarization. Also, the thermal radiation spectrum shifts to a higher frequency, and in contrast to the TE mode, as the angle increases, the width of the thermal radiation spectrum reduces. For example, the maximum radiation width is about 1.02 THz at $\theta = 30°$, and it lessens to about 0.64 THz at $\theta = 85°$. The width of the omnidirectional spectrum of thermal radiation in this case occurs at frequencies of about $f_a = 4.26$ THz and $f_b = 4.39$ THz, which remained invariant in the related frequency range for TM polarization, meaning the thermal radiation spectrum will be always in its maximum magnitude. However, it is clear that a narrower width ($\Delta f = 0.13$ THz) occurred compared to the TE mode. Generally, the impacts of TE and TM modes on the transmission, reflection, radiation quantities, and PBG depend on the proposed structure, materials, and incident angle of the THz waves. In the case of our study, according to our calculations, the proposed structure shows more tunability towards the TM polarization mode for some parameters. For instance, the radiation PBGs in the TE mode considerably shift faster towards higher frequencies than in the TE mode by increasing the angle of incidence.

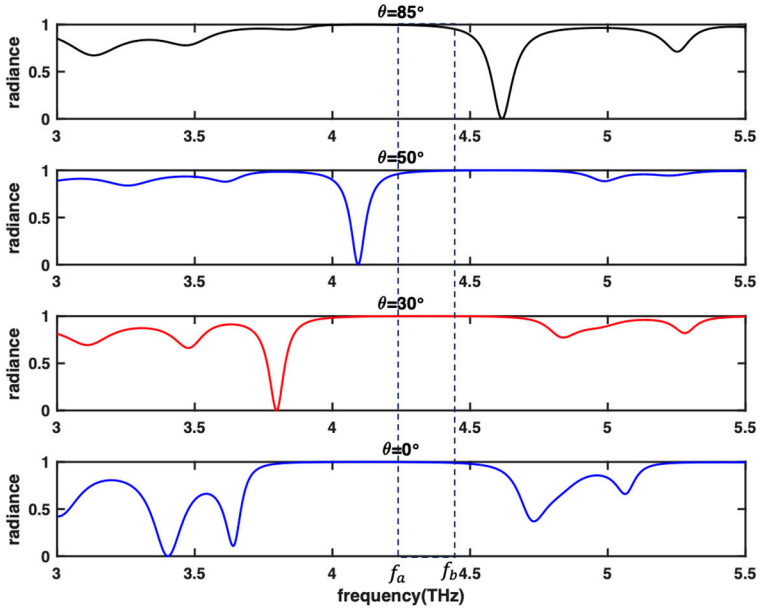

Figure 4. Thermal radiation power spectrum (dashed rectangle depicts the omnidirectional spectrum) of the 1D MQP PC (with FB and ML sequences) as a function of frequency for TM polarization at T = 300 K and M = 1, under several incident angles $\theta = 0°$, 30°, 50°, and 85°. Here, the lattice constants are considered $d_A = 12$ µm, $d_B = 6$ µm, $d_C = 8$ µm, and $d_D = 6$ µm.

3.4. Total Period Number

Current research in thermal radiation manipulation using periodic structures is focused on two main areas. The first is to create highly selective narrow-band thermal emitters with wavelength, directional, and polarization selectivity. These emitters hold promise for applications in IR sensors and various IR sources. Secondly, researchers are exploring the use of PCs to design wide-band thermal emitters that exhibit near-black-body thermal emission within a specific wavelength range while significantly reducing emissions outside that range. The primary driving forces behind advancements in broadband selective thermal emitters include applications in thermophotovoltaic energy conversion, solar–thermophotovoltaic conversion, and solar absorbers/reflectors. Consequently, changing M is one of the ways to control the bandwidths of thermal radiation in the desired frequency ranges. The optimization of transmittance loss bandwidth serves as a pivotal performance parameter for such multilayer structures (THz filters, thermal emitters). The aim is to achieve a more refined bandwidth, thereby enhancing the quality factor (Q) for narrow band filters. This sought-after enhancement can be effectively realized through the strategic augmentation of the periodic number M. In order to study the effect of the changes in total period number M on thermal radiation, several period numbers are applied to the structure. As shown in Figure 5, the thermal radiation spectrum is plotted for $M = 1$, 3, and 5 for the TE mode. Thermal radiation fluctuations increase within a specific frequency range as the period number M increases. As a result of increasing M, desirable band-gaps and peaks occur. Furthermore, the number of periods can be changed to tailor the position of the band-gaps. As M increases, the width of the PBGs decreases and switches to higher frequencies, as shown in the figure. However, these changes are so minor that they may be negligible. In general, the width of these gaps is proportional to the period number in the opposite direction. As a result, the number of periods has a significant impact on how band-gaps are configured and adjusted. In the preceding calculations, the loss in the semiconductor material InSb has been omitted. In practical applications, however, losses in the semiconductor material are unavoidable. The introduction of losses invariably results in the degradation of the filter's performance.

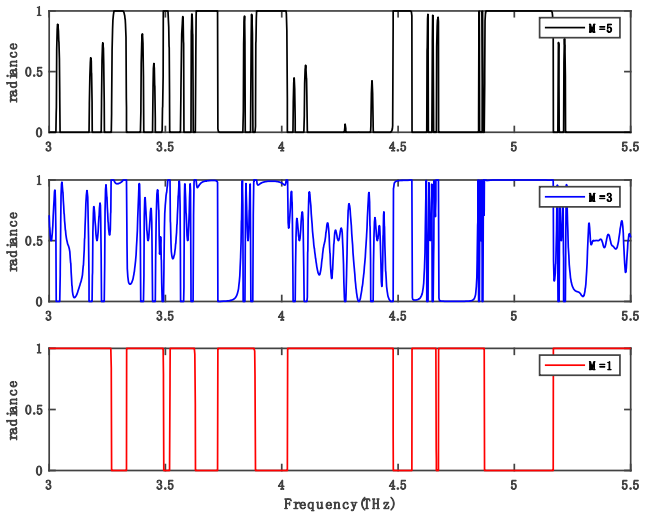

Figure 5. The thermal radiation power spectrum of 1D MQP PC (with FB and ML sequences) as a function of frequency at T = 300 K, under several numbers of periods M = 1, 3, and 5, for TE mode. Here, thicknesses of the layers are considered as $d_A = 28$ μm, $d_B = 12$ μm, $d_C = 3$ μm, and $d_D = 12$ μm.

4. Conclusions

The thermal radiation spectrum of the suggested structure has been evaluated under different circumstances at various frequency ranges in order to control the thermal radiation spectrum and evaluate its tunability. The use of an MQP arrangement in tuning thermal radiation, which provides a wider degree of freedom in structural design compared to periodic and quasi-periodic arrangements, is the fundamental distinction between this work and other investigations. An adjustable THz filter for both s and p polarization was produced as a result of the suggested structure's ability to allow THz waves to propagate. The tunability of THz filters the proposed structures and offers practical advantages in tailoring the transmission characteristics of THz waves which exhibit unique and adjustable properties, allowing for precise control of the filter's response in the THz frequency range. Tunability is achieved by manipulating the different parameters like thickness of layers, number of layers, the utilized materials, and the angle of incident. When the angle of incidence changes, both the maximum thermal radiation spectrum and the bandwidth of the PBGs can be adjusted. In terms of the highest amount of thermal radiation, it was discovered that the structure produces a sufficient omnidirectional spectrum. The manipulation of the period number also affects the control of band-gaps and thermal radiation spectra. As the periods increase, well-behaved peaks and PBGs form in the transmission and thermal radiation spectrum. To name a few applications in the THz region, the proposed structure can be used to improve THz filters, sensors, thermal antennas, and selective thermal emitters.

Author Contributions: Conceptualization, A.M., A.B. and M.P.; Methodology, A.M.; Software, A.M.; Validation, A.K. and M.P.; Formal analysis, A.M. and A.B.; Investigation, A.M. and A.K.; Resources, A.K., A.B. and M.P.; Writing—original draft, A.M.; Writing—review & editing, A.M. and A.K.; Visualization, A.M. and A.B.; Supervision, A.K.; Project administration, A.K. All authors have read and agreed to the published version of the manuscript.

Funding: This research received no external fundings.

Data Availability Statement: The data presented in this study are available on request from the corresponding author. The data are not publicly available due to privacy.

Conflicts of Interest: The authors declare no conflict of interest.

References

1. Yablonovitch, E. Inhibited spontaneous emission in solid-state physics and electronics. *Phys. Rev. Lett.* **1987**, *58*, 2059. [CrossRef]
2. John, S. Strong localization of photons in certain disordered dielectric superlattices. *Phys. Rev. Lett.* **1987**, *58*, 2486. [CrossRef]
3. Tang, G.J.; He, X.T.; Shi, F.L.; Liu, J.W.; Chen, X.D.; Dong, J.W. Topological photonic crystals: Physics, designs, and applications. *Laser Photon. Rev.* **2022**, *16*, 2100300. [CrossRef]
4. Christensen, T.; Po, H.C.; Joannopoulos, J.D.; Soljačić, M. Location and topology of the fundamental gap in photonic crystals. *Phys. Rev. X* **2022**, *12*, 021066.
5. Han, W.; Qing, X.; Fangzhou, O. One-way two-dimensional photonic crystal absorber combined with graphene. *J. Opt.* **2023**, *52*, 339–346. [CrossRef]
6. Chen, Z.; Shiomi, J.; Hu, R. Multi-band nonreciprocal thermal radiation via the coupling effect of tamm Plasmon and defect mode. *SSRN Electron. J.* **2023**, *210*, 4374467.
7. Purcell, E.M. Spontaneous emission probabilities at radio frequencies. *Phys. Rev.* **1946**, *69*, 839.
8. Maksimovic, Z.; Jaksic, M. Modification of thermal radiation by periodical structures containing negative refractive index metamaterials. *Phys. Lett. A* **2005**, *342*, 497–503. [CrossRef]
9. Cornelius, C.M.; Dowling, J.P. Modification of planck blackbody radiation by photonic band-gap structures. *Phys. Rev. A* **1999**, *59*, 4736–4746. [CrossRef]
10. Singhal, V.; Zhu, J.; Song, J.; Wang, H.; Bermel, P. Tri-phase photonic crystal emitter for thermophotovoltaic systems. *Appl. Phys. Lett.* **2023**, *123*, 131101. [CrossRef]
11. Florescu, M.; Busch, K.; Dowling, J. Thermal radiation in photonic crystals. *Phys. Rev. B* **2007**, *75*, 20110. [CrossRef]
12. Lee, B.J.; Fu, C.J.; Zhang, Z.M. Coherent thermal emission from one-dimensional photonic crystals. *Appl. Phys. Lett.* **2005**, *87*, 071904. [CrossRef]
13. Sharma, Y.; Aman, A.; Prasad, S.; Singh, V. Properties of thermal radiation power spectra in truncated one-dimensional photonic crystals. *Opt. Quantum Electron.* **2017**, *49*, 341. [CrossRef]
14. Costa, C.H.; Vascocselos, M.S.; Fulco, U.L.; Albuquerque, E.L. Thermal radiation in one-dimensional quasicrystals with graphene. *Opt. Mater.* **2017**, *72*, 756–764. [CrossRef]
15. He, Y.; Guo, L.; Li, J.; Chen, Y.; Yin, C. Thermal emission of one-dimensional conjugated photonic crystals heterojunction embedded with graphene. *Eur. Phys. J. B* **2019**, *92*, 63. [CrossRef]
16. Han, J.; Lakhtakia, A. Semiconductor split-ring resonators for thermally tunable terahertz metamaterials. *J. Mod. Opt.* **2008**, *56*, 554–557. [CrossRef]
17. Zhu, Z.; Shi, C.; Liu, Y.; Zhang, D.; Wang, Q.; Du, Q.; Dong, X.; Li, S.; Wang, W. Enhanced performance of organic light-emitting diodes by integrating quasi-periodic micro-nano structures. *Spectrochim. Acta A* **2023**, *292*, 122401. [CrossRef]
18. Oskouei, S.B.; Bayer, Ö. Experimental and numerical investigation of melting and solidification enhancement using Fibonacci-inspired fins in a latent thermal energy storage unit. *Int. J. Heat Mass Transf.* **2023**, *210*, 124180. [CrossRef]
19. Ramakrishna, S.A. Physics of negative refractive index materials. *Rep. Prog. Phys.* **2005**, *68*, 449. [CrossRef]
20. Shalaev, V.M. Optical negative-index metamaterials. *Nat. Photonics* **2007**, *1*, 41–48. [CrossRef]
21. Wu, F.; Lu, G.; Guo, Z.; Jiang, H.; Xue, C.; Zheng, M.; Chen, C.; Du, G.; Chen, H. Redshift gaps in one-dimensional photonic crystals containing hyperbolic metamaterials. *Phys. Rev. Appl.* **2018**, *10*, 064022. [CrossRef]
22. Xia, J.; Chen, Y.; Xiang, Y. Enhanced spin Hall effect due to the redshift gaps of photonic hypercrystals. *Opt. Express* **2021**, *29*, 12160–12168. [CrossRef]
23. Wu, F.; Chen, M.; Xiao, S. Wide-angle polarization selectivity based on anomalous defect mode in photonic crystal containing hyperbolic metamaterials. *Opt. Lett.* **2022**, *47*, 2153–2156. [CrossRef]
24. Padilla, W.J.; Dimitri, N.B.; Smith, D.R. Negative refractive index metamaterials. *Materialstoday* **2006**, *9*, 28–35. [CrossRef]
25. Luan, P.-G. Metamaterials and transformation optics. In *The Current Trends of Optics and Photonics*; Springer: Dordrecht, The Netherlands, 2014; pp. 35–58.
26. Baseri, A.; Keshavarz, A. Designing a double-negative metamaterial photonic crystal using the Thue-Morse sequence. *J. Comput. Electron.* **2022**, *21*, 270–279. [CrossRef]
27. Baseri, A.; Keshavarz, A.; Hatef, A. A type of arrangement for photonic crystal structures interacting with a Terahertz wave with omnidirectional and thermal effects. *J. Appl. Phys.* **2020**, *127*, 214304. [CrossRef]
28. King, P.D. Acoustic Properties of Periodically and Quasi-Periodically Modulated Waveguides. Master's Thesis, University of Salford, Manchester, UK, 2006.
29. Sukhoivanov, I.A.; Guryev, I.V. *Photonic Crystals: Physics and Practical Modeling*; Springer: Berlin/Heidelberg, Germany, 2009; Volume 152.
30. Scott, C. *The Spectral Domain Method in Electromagnetics*; Norwood: Artech House, MA, USA, 1989.
31. Hashemi, A.R.; Farzad, M.H.; Montakhab, A. Effect of Positional Disorder on Transmissional Properties of a Two-Dimensional Photonic Crystal: An FDTD Study. *arXiv* **2009**, arXiv:0909.1022.
32. Lucio, V.; Cicchetti, R.; Capece, P. Spectral dyadic Green's function formulation for planar integrated structures. *IEEE Trans. Antennas Propag.* **1988**, *36*, 1057–1065.
33. Li, Y.; Xiang, Y.; Wen, S.; Yong, J.; Fan, D. Tunable terahertz-mirror and multi-channel terahertz-filter based on one-dimensional photonic crystals containing semiconductors. *J. Appl. Phys.* **2011**, *110*, 073111. [CrossRef]

34. Arvind, N.; Chen, G. Thermal radiation in 1D photonic crystals. In *Radiative Transfer-IV. Fourth International Symposium on Radiative Transfer*; Begel House Inc.: Danbury, CT, USA, 2004.
35. Pigeat, P.; Rouxel, D.; Weber, B. Calculation of thermal emissivity for thin films by a direct method. *Phys. Rev. B* **1998**, *57*, 9293. [CrossRef]
36. Iván, H.D.; Ruiz, A.C.; Raffi, L.M.G.; Romero-García, V. Matrix formulation in Acoustics: The transfer matrix method. *Model. Sci. Educ. Learn.* **2019**, *12*, 153–164.
37. Rui, X.; Wang, X.; Zhou, Q.; Zhang, J. Transfer matrix method for multibody systems (Rui method) and its applications. *Sci. China Technol. Sci.* **2019**, *62*, 712–720. [CrossRef]
38. Moharam, M.G.; Gaylord, T.K. Three-dimensional vector coupled-wave analysis of planar-grating diffraction. *J. Opt. Soc. Am.* **1983**, *73*, 1105–1112. [CrossRef]
39. Sergey, S.; Shcherbakov, A.A. Reformulated Fourier Modal Method with improved near field computations. *J. Comput. Sci.* **2023**, *67*, 101936.
40. Shen, H.; Wang, Z.; Wu, Y.; Yang, B. One-dimensional photonic crystals: Fabrication, responsiveness and emerging applications in 3D construction. *RSC Adv.* **2016**, *6*, 4505–4520. [CrossRef]
41. Marie, D.; Jiménez-Solano, A.; Lotsch, B.V. Stimuli-responsive one-dimensional photonic crystals: Design, fabrication and sensing. *Mater. Adv.* **2022**, *3*, 7406–7424.
42. Yang, M.K.; French, R.H.; Tokarsky, E.W. Optical properties of Teflon®AF amorphous fluoropolymers. *J. Micro/Nanolithography MEMS MOEMS* **2008**, *7*, 033010. [CrossRef]
43. Krishna, M.; Ghanashyam, K.; Narasimha, R.; Mohan, S. Structural and optical properties of zirconia thin films. *Thin Solid Films* **1990**, *193*, 690–695. [CrossRef]
44. Withayachumnankul, W.; Abbott, D. Metamaterials in the Terahertz Regime. *IEEE Photonics J.* **2009**, *1*, 99–118. [CrossRef]
45. Mu, Q.; Fan, F.; Chen, S.; Xu, S.; Xiong, C.; Zhang, X.; Wang, X.; Chang, S. Tunable magneto-optical polarization device for terahertz waves based on InSb and its plasmonic structure. *Photonics Res.* **2019**, *7*, 325–331. [CrossRef]
46. Yoshinaga, H.; Oetjen, R.A. Optical Properties of Indium Antimonide in the Region from 20 to 200 Microns. *Phys. Rev.* **1956**, *101*, 526. [CrossRef]
47. Zhang, L.; Zhang, Y.; He, L.; Wang, Z.; Li, H.; Chen, H. Zero-bar n gaps of photonic crystals consisting of positive and negative index materials in microstrip transmission lines. *J. Phys. D Appl. Phys.* **2007**, *40*, 2579. [CrossRef]
48. Howells, S.C.; Schlie, L.A. Transient terahertz reflection spectroscopy of undoped InSb from 0.1 to 1.1 THz. *Appl. Phys, Lett.* **1996**, *69*, 550–552. [CrossRef]
49. Florescu, M.; Lee, H.; Stimpson, A.J.; Dowling, J. Thermal emission and absorption of radiation in finite inverted-opal photonic crystals. *J Phys. Rev. A.* **2005**, *72*, 033821. [CrossRef]
50. Pendry, J.B.; Holden, A.J.; Robbins, D.J.; Stewart, W.J. Low frequency plasmons in thin-wire structures. *J. Phys. Condens. Matter* **1998**, *10*, 4785–4809. [CrossRef]
51. Liang, Y.; Lin, H.; Lin, S.; Wu, J.; Li, W.; Meng, F.; Yang, Y.; Huang, X.; Jia, B.; Kivsha, Y. Hybrid anisotropic plasmonic metasurfaces with multiple resonances of focused light beams. *Nano Lett.* **2021**, *21*, 8917–8923. [CrossRef]